Mechanical Systems and Signal Processing 100 (2018) 135–151

Contents lists available at ScienceDirect

Mechanical Systems and Signal Processing

journal homepage: www.elsevier.com/locate/ymssp

Analytical study of a quasi-zero stiffness coupling using a torsion magnetic spring with negative stiffness

Yisheng Zheng, Xinong Zhang *, Yajun Luo, Yahong Zhang, Shilin Xie

State Key Laboratory for Strength and Vibration of Mechanical Structures, Xi'an Jiaotong University, Xi'an 710049, PR China

ARTICLE INFO

Article history:
Received 4 December 2016
Received in revised form 14 July 2017
Accepted 16 July 2017
Available online 26 July 2017

Keywords:
Torsion isolator
Quasi-zero stiffness
Negative stiffness
Magnetic spring

ABSTRACT

By now, many translation quasi-zero stiffness (QZS) mechanisms have been proposed to overcome the restriction between the isolation frequency range and the load bearing capacity of linear isolators. The couplings of rotor systems undertake the functions of transmitting static driving torque and isolating disturbing torque simultaneously, which creates the demand of torsion QZS mechanisms. Hence a QZS coupling is presented in this paper, where a torsion magnetic spring (TMS) composed of two coaxial ring magnet arrangements in repulsive configuration is employed to produce negative torsion stiffness to counteract the positive stiffness of a rubber spring. In this paper, the expressions of magnetic torque and stiffness are given firstly and verified by finite element simulations; and the effect of geometric parameters of the TMS on its stiffness characteristic is analyzed in detail, which contributes to the optimal design of the TMS. Then dynamic analysis of the QZS coupling is performed and the analytical expression of the torque transmissibility is achieved based on the Harmonic Balance Method. Finally, simulation of the torque transmissibility is carried out to reveal how geometric parameters of the TMS affect the isolation performance.

© 2017 Published by Elsevier Ltd.

1. Introduction

Negative-stiffness mechanism (NSM) is relative to the phenomenon of instability, which is generally avoided in the design of mechanical structures. However, the concept of negative stiffness has acquired much attention recently due to its smart applications in areas such as material damping and stiffness, energy harvesting, vibration absorber and vibration isolator. Lakes [1,2] firstly studied composites that can have extreme damping by embedding negative-stiffness inclusions in a matrix. Jaglinski and Lakes [3] further claimed that composite materials with negative-stiffness inclusions would possess extreme stiffness greater than diamond. Dong and Lakes [4] proposed an advanced damper that can achieve high structural damping and high stiffness simultaneously by employing negative-stiffness elements. Haberman and his group presented a negative-stiffness metamaterial relied on the small-scale buckling elements, the macroscopic stiffness and loss of which are theoretically investigated [5,6]. Actually, most NSM present negative stiffness only in a limited displacement range, which means that the structures can still be stable beyond this range and usually two stable states can be attained. Hence NSM are often harnessed to design bistable systems, which are especially beneficial in energy harvesting due to its snap-through property [8]. There are abundant researches studying bistable energy harvesting systems in recent years; thorough review can be referred in [7,8]. Besides, bistable systems are also beneficial in improving vibration absorbing performance.

* Corresponding author.
E-mail addresses: zhysh966@163.com (Y. Zheng), xnzhang@mail.xjtu.edu.cn (X. Zhang).

http://dx.doi.org/10.1016/j.ymssp.2017.07.028
0888-3270/© 2017 Published by Elsevier Ltd.

Avramov [9,10] firstly studied a snap-through truss as an absorber for linear oscillators. Johnson [11] studied the disturbance cancellation performance of a bistable element attached to a linear oscillator. Manevitch [12] and Remeo [13] investigated the target energy transfer phenomenon of a linear oscillator with light bisatable attachment, and proved that the bistable attachment can be efficient absorbers and dissipaters of impulsively induced vibration energy. In the area of vibration absorbers, negative stiffness also attracts attention from researchers. Yao [14] investigated a low frequency vibration absorber combining positive stiffness and negative stiffness for rotor systems. Zhao [15] designed a low-frequency membrane acoustic metamaterial absorber by employing magnetic negative stiffness. In order to reduce the bandgap frequency of periodic structures, Zhou [16] presented a high-static-low-dynamic stiffness resonator. Weber [17] presented an adaptive tuned mass damper with magnetorheological material, which can produce negative stiffness. In these literatures, negative stiffness is utilized to reduce the resonance frequency of absorbers. Besides, Shen [18,19] proposed a kind of dynamic vibration absorber with negative stiffness and demonstrated that it can broaden the efficient frequency range of vibration mitigation. Acar [20] employed NSM to adjust the tension of a string-mass absorber and hence its resonance frequency, so as to realize an adaptive absorber. In the area of vibration isolators, negative stiffness is studied a lot; because the resonance frequency is a crucial factor to isolation performance and NSM is quite effective in reducing stiffness. Since the topic of this paper is about vibration isolation, the application of NSM in isolation would be introduced thoroughly in the following.

The isolation frequency range of linear isolators starts from $\sqrt{2}$ times of its resonance frequency, thus methods to reduce the resonance frequency can be employed to expand the isolation frequency band. But the disadvantage is that the static deflection of the linear isolator will be very large if the resonance frequency is reduced to a quite low level. This is why the quasi-zero stiffness (QZS) isolator is investigated by researchers, which possesses the advantage of high-static stiffness and low-dynamic stiffness and thus could reduce the resonance frequency while maintaining small static deformation. The main way to realize QZS is to connect the positive-stiffness elastic element with the negative-stiffness mechanism (NSM) in parallel and many NSM have been proposed so far. Platus [21] employed two pre-stressed bars to produce negative stiffness. Such a mechanism has also been used to design QZS isolators by Huang [22,23] and Liu [24]; and both vibration isolation performance and shock isolation performance are studied. Carrela et al. [25,26] utilized inclined springs to generate negative stiffness to cancel the positive stiffness of a vertical spring; and the static and dynamic characteristic of such a system was fully studied. Le et al. [27,28] employed the same NSM to design a QZS isolator for vehicle seats. Lan [29] also studied this kind of QZS isolator and further proposed an adjusting mechanism to handle a wide range of loads. Xu [30] presented a similar QZS mechanism with four oblique springs and one vertical spring. Besides, utilizing magnets to produce negative magnetic stiffness is also an effective way to realize QZS characteristic. If three magnets are arranged in an attractive configuration in the vertical direction, negative stiffness could be generated; Carrela [31] and Shin [32] studied such a NSM and designed a QZS isolator. Zhou [33] developed a QZS isolator using two electromagnetic magnets and a permanent magnet to produce negative stiffness. Installing three cuboidal permanent magnets in repulsive configuration is also a way to produce negative stiffness [34]; based on this mechanism, Shan [35] further developed a QZS isolator using two ring magnet arrangements to provide negative stiffness for a pneumatic spring. In our previous work [36], a negative stiffness magnetic spring composed of two ring permanent magnets that are radially magnetized was proposed to design a translation QZS isolator. Moreover, to avoid the difficulty of manufacturing ring magnets with radial magnetization, the alternative way using tile magnets magnetized uniformly to replace the ring magnets was investigated in [36]. There are also other researchers utilizing the inherent nonlinearity of materials or inherent nonlinearity of restoring force of structures to design QZS isolators, rather than the mechanism with positive-stiffness element and negative-stiffness element connected in parallel. Araki [37] applied a newly developed superplastic Cu-Al-Mn shape memory alloy bar to design a QZS mechanism, which had the advantage of large loading capacity and large stroke length. Robertson analyzed a type of magnetic levitation system which has nonlinear force vs. displacement characteristic and exhibits localized zero stiffness in [38]; a six-degree-of-freedom QZS magnetic levitation was further designed and tested by his group [39]. Other designs to yield QZS characteristic include the scissor-like structure by Sun [40] and the cam-roller-spring mechanism by Zhou [41].

Though the literatures about quasi-zero stiffness isolators are abundant, most of them discuss translation QZS isolators and there are barely any investigating torsion QZS isolators. The torsion vibration is a serious problem for rotating machinery; excessive torsion vibration can result in gear tooth failure, gear wear and shaft broken. Thus it is greatly significant to design torsion isolators with high isolation performance. A torsion isolator for the rotating machinery is actually can be seen as a coupling to connect two shafts because it also undertakes the function of transmitting the driving torque. Hence, the name *QZS coupling* is equivalent to *torsion QZS isolator* in this paper. Ideally, the driving torque is static and it can be transmitted through the coupling without any harm. But if the disturbing torque exists, it could also be transmitted to the driven shaft through the coupling and hence influence the working performance of rotor systems. Similar to translation isolators, the isolation frequency band of torsion isolators can be increased if its stiffness is decreased, accompanied by the problem that the static torsion deformation due to the static driving torque component will be large if the stiffness approaches a low level. Thus designing a coupling with the characteristic of high static low dynamic stiffness is necessary. By now, only one literature [42] has ever studied the torsion QZS isolator, where the pre-compressed cam-roller mechanism is designed to provide negative torsion stiffness to counteract the positive torsion stiffness of the vulcanized rubber between shafts. The main disadvantage of such a design is that the structure is complicated and the size of the coupling can be too large for application in the industry.

In this paper, a novel torsion magnetic spring (TMS) with negative stiffness is proposed. The mechanism is composed of two coaxial ring magnet arrangements in repulsive configuration and each ring magnet arrangement is comprised of several tile magnets magnetized radially. The proposed TMS is installed in parallel with a rubber spring to counteract its positive stiffness and hence the torsion QZS stiffness characteristic can be achieved. Actually, similar mechanisms have been investigated as magnet couplings for many years [43–46]. Distinguished from the application discussed in this paper, they are in attractive configuration rather than repulsive configuration and are employed to supply driving torque without considering the functionality of isolating disturbing torque. Considering that much research work has been done on this kind of magnet coupling, much existing experience and results can be utilized in designing a TMS with negative stiffness for the QZS coupling as proposed in this paper. The advantage of such a QZS coupling is that it is compact and can maintain a relatively small size comparing to the torsion QZS isolator presented in [42].

The paper is organized as follows. In Section 2, the schematic model of the QZS coupling is illustrated and the analytical expressions of the magnetic torque and stiffness are given and verified. In Section 3, the effect resulted from geometric parameters of the torsion magnetic spring on its stiffness characteristic is analyzed. In Section 4, dynamic analysis of the QZS coupling is performed and the torque transmissibility is studied. Finally, some conclusions are summarized in Section 5.

2. The quasi-zero stiffness (QZS) coupling

2.1. Model of the QZS coupling

The schematic of the QZS coupling is shown as Fig. 1. The tooth-type rubber spring, shown as Fig. 1(b), connects the driving shaft and the driven shaft, which possesses positive torsion stiffness. The torsion magnetic spring (TMS), as shown in Fig. 1(c), that can generate negative torsion stiffness is composed of two ring magnet arrangements: the outer one is fixed with the driving shaft while the inner one is connected with the driven shaft. The bearings are employed to restrict the axial and radial motion of the shafting system. When the motor rotates, the relative angular displacement between the driving shaft and driven shaft would lead to production of torque of the rubber spring and TMS and then the rotor will be driven.

As depicted Fig. 1(c), the TMS is assembled with tile magnets. The inner ring magnet arrangement and the outer one have the same even number of tile magnets, which are magnetized radially and the magnetization direction varies alternately

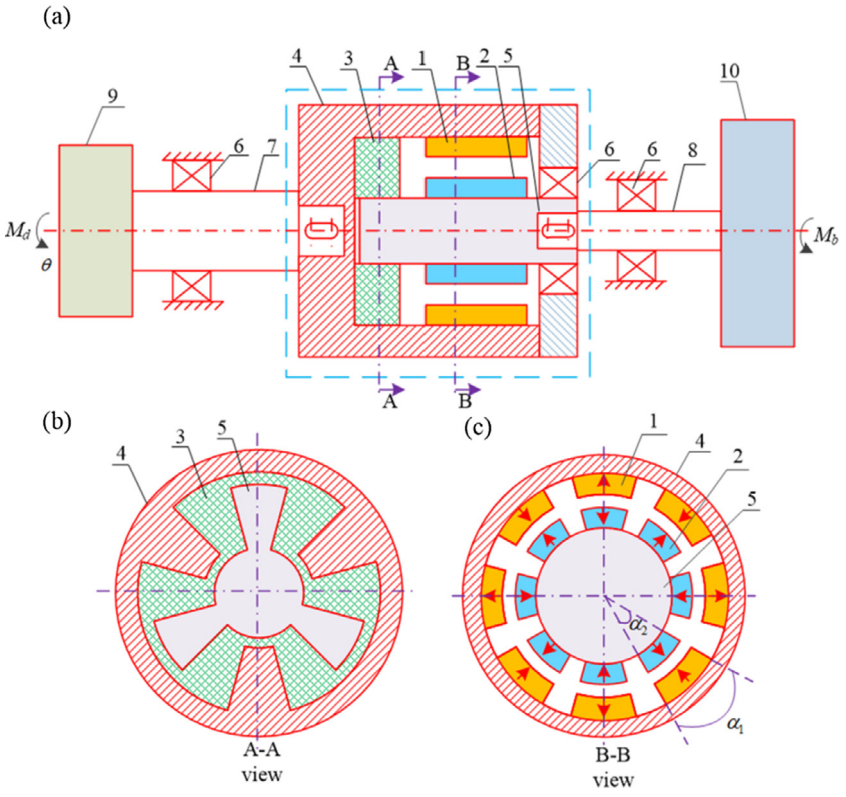

Fig. 1. (a) Schematic of the QZS coupling (the components in the dashed box compose the coupling); (b) A-A view is the cross-section view of the rubber spring; (c) B-B view is the cross-section view of the TMS (torsion magnetic spring): 1-outer magnet arrangement of the TMS; 2-inner magnet arrangement of the TMS; 3-rubber spring; 4,5-connectors; 6-bearing; 7-driving shaft; 8-driven shaft; 9-motor; 10-rotor.

along the circumference. Actually, negative stiffness can also be produced if all the tile magnets of the inner ring magnet arrangement (and the outer one) are magnetized towards the same direction. However, the strong repulsive force produced between adjacent tile magnets will make it difficult to install the tile magnets. This is why the alternative magnetization directions are designed for the tile magnets. When the two magnet arrangements stay at such a state that the inner tile magnets face the outer ones directly and their magnetization directions are opposite, just as illustrated in Fig. 1(c), it can be known that the TMS is in repulsive configuration and unstable in the torsion direction and thus it could produce negative torsion stiffness. On the other hand, the magnetic torque at this state is zero due to the axial symmetry. The characteristic of such a TMS is very similar to that of the translation negative-stiffness mechanisms. Hence, it is natural for us to employ such a TMS to design a torsion QZS coupling. The QZS coupling could supply large driving torque with the driven shaft while avoiding transmitting the disturbing torque to it.

The state shown in Fig. 1(c) is an ideal operating position for the QZS coupling when the shaft system is in operation. At this position, the total driving torque of the coupling is provided by the rubber spring only and the torque of the TMS is zero. Assuming that the relative angular displacement between the inner magnet arrangement and the outer one is θ_0 when the rubber spring is undeformed, the driving shaft should be rotated by θ_0 relative to the driven shaft and then comes to this ideal operating point. Thus the total driving torque that the rubber spring provides at this point is $K_r\theta_0$, where K_r is the stiffness of the rubber spring and is supposed to be constant when the angular displacement θ of the QZS coupling is small. The term $K_r\theta_0$ should balance the static driving torque that the rotor system demands rightly, which means that this operating point is the equilibrium position of the QZS isolator. If the required static driving torque deviates from $K_r\theta_0$, the isolation performance of the QZS coupling will be deteriorated because the equilibrium position drifts away from the position where the lowest stiffness is. This problem is called "load imperfection", which has been discussed in [47,48] for translation QZS isolators, and some mechanisms [29,49] are also proposed to solve this problem. For the QZS coupling under different working conditions, the static driving torque can be varied; for example, if the coupling is employed in the drive chain of a car, the driving torque depends on the speed of the car. Hence a mechanism to adjust the QZS coupling to ensure that it is always operated at the ideal position need to be developed in the future.

Assuming that the torsion stiffness of the TMS is $K_m(\theta)$, the total restoring stiffness of the coupling is then presented as

$$K(\theta) = K_r + K_m(\theta) \tag{1}$$

Accordingly, the total restoring torque of the coupling is given as

$$M(\theta) = K_r\theta - M_m(\theta) \tag{2}$$

where $M_m(\theta)$ is the magnetic torque and its opposite number is the contribution to the restoring torque of the coupling.

2.2. Magnetic torque and stiffness of the torsion magnetic spring (TMS)

The main component of the QZS coupling that need to be specially designed is the TMS. In order to design the TMS, the magnetic force and stiffness should be calculated. Firstly, geometric parameters of the TMS are defined, just as shown in Fig. 2. It is notable that since space exists between adjacent tile magnets, two parameters expressing the angular width of the tile magnets are given, presented as $\lambda_1 = N\alpha_1/2\pi, \lambda_2 = N\alpha_2/2\pi$. N is the number of poles of the outer magnet arrange-

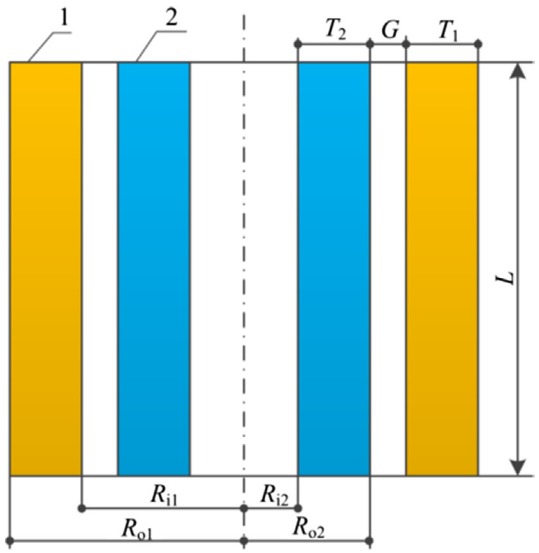

Fig. 2. Longitudinal-section view of the torsion magnetic spring (TMS).

ment (or the inner one); α_1 and α_2 are the angular width of the outer tile magnet and inner tile magnet respectively. If $\lambda_i = 1$ $(i = 1, 2)$, no space exists between adjacent tile magnets.

Such a configuration of magnets has ever been studied as magnet couplings and all kinds of methods have been proposed to calculate its torque [44–46]. Here in this paper, the analytical expression of magnetic torque given in [46] is employed, which is derived based on the Coulombian model. The detailed expression of the magnetic torque $M_m(\theta)$ is given in Appendix A. In order to design the QZS coupling, the stiffness characteristic of the TMS should be obtained and analyzed, which can be derived based on $M_m(\theta)$ and also presented in Appendix A.

Before detailed analysis of the magnetic torque and stiffness of the TMS, the correctness of the analytical formulation of magnetic torque in Appendix A is validated. Here the finite element software ANSYS will be employed to calculate the magnetic torque. The geometric model in the finite element simulation is comprised of a magnetic coupling and the air surrounding it. The meshing model of the magnetic coupling is shown in Fig. 3(a), whereas that of the air is not shown. The element type of both magnets and air is SOLID236. When the relative angular displacement between inner tiles and outer tiles is zero, the magnetic flux density in the area of magnets is shown in Fig. 3(b). The obtained magnetic torque is shown in Fig. 4(a) and compared with the analytical solution, which shows that the results achieved by these two methods have good coincidence and hence demonstrates the correctness of the analytical formulations in Appendix A.

As shown in Fig. 4, a case study is done to clearly illustrate the torque and stiffness characteristic of the TMS. It shows that the magnetic torque and stiffness are symmetric about the equilibrium position, which is predictable due to the symmetry of the configuration of magnets. At the equilibrium position, i.e. where the relative angular displacement between the two ring magnet arrangements is zero, the magnetic torque is zero and the magnetic stiffness is negative, which is just what needed to realize the QZS characteristic. As shown in Fig. 4(b), it is a disadvantage that the magnetic stiffness about the equilibrium position exhibits strong nonlinearity, which is not fit for designing the QZS coupling because it will result in large jump-down frequency. However, the stiffness characteristic can be optimized by choosing appropriate geometric parameters of the TMS, which will be analyzed in Section 3.

3. Effect of geometric parameters of the torsion magnetic spring (TMS) on its torsion stiffness

When designing a quasi-zero stiffness (QZS) coupling, three objectives need to be attained: firstly, the total stiffness about the equilibrium position should be low since lower stiffness could lead to lower resonance frequency; secondly, the stiffness about the equilibrium position should has weak nonlinearity because strong nonlinearity can result in jumping phenomenon; thirdly, the effective stroke length where the QZS coupling works well need to be large enough. The effective stroke length is actually relative to the nonlinearity of stiffness: the weaker the nonlinearity is, the larger the effective stroke length will be.

Geometric parameters of the magnets can affect the stiffness characteristic of the TMS, which will be analyzed in this section in order for optimal design of the TMS. The following geometric parameters will be evaluated: number of poles (N); parameters characterizing the angular width of tile magnets (λ_1 and λ_2); air gap between the inner magnet and the outer one (G); inner radii of inner tiles (R_{i2}), radial thickness (T_1 and T_2) and length (L) of tile magnets. For a coupling working at the stable state, the relative angular displacement between the inner magnet and outer magnet due to the disturbing torque is small and hence only the magnetic stiffness in a small region about the equilibrium position need to be considered. Here the magnetic stiffness in the half period around the equilibrium position will be analyzed.

3.1. Effect of the number of poles (N)

It can be seen from Fig. 5 that increasing the number of poles can improve the negative stiffness at the equilibrium position until that N reaches a certain value. If N is excessively large, e.g. when N increases from 16 to 18, the magnetic stiffness of the equilibrium point will decrease instead. Hence the number of poles should be well chosen to gain large negative stiffness. Another factor that needs to be considered when choosing the number of poles is the process of mounting. It would be quite troublesome to mount the tile magnets if the number of poles is too large. As for the case in this section, setting the number of poles to be 12 is appropriate to some extent since it can produce large negative stiffness (though not the largest) while keeping the structure simple.

3.2. Effect of the angular width of tile magnets (λ_1 and λ_2)

The effect of angular width of tile magnets on the stiffness characteristic is illustrated in Fig. 6. In this section, the number of poles N is set to be constant. Thus the angular width is only affected by parameters λ_1 and λ_2. Two situations are considered: (1) the angular width of inner tiles and that of outer tiles vary simultaneously and keep the same, as shown in Fig. 6(a); (2) there is a difference between the angular width of inner tiles and that of outer tiles and the difference varies, as shown in Fig. 6(b). Fig. 6(a) shows that increasing the angular width can increase negative stiffness, while Fig. 6(b) shows that increasing the difference of angular width would make the stiffness around the equilibrium position more uniform. This enlightens us that though the largest negative stiffness can be achieved when $\lambda_1 = 1$ and $\lambda_2 = 1$, it is better to reduce one of them so as

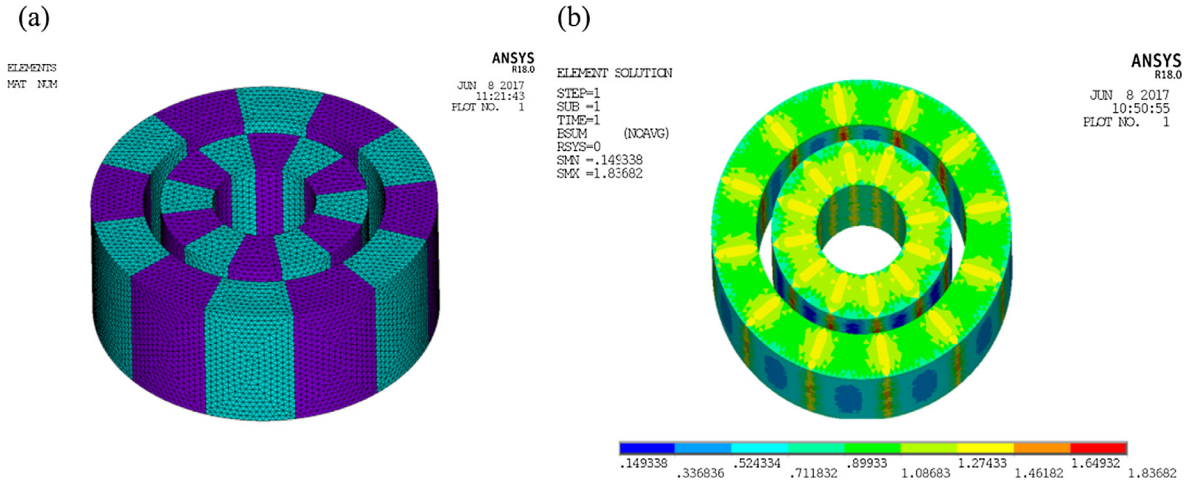

Fig. 3. (a) Meshing model of the magnetic coupling (different colors represent different magnetization directions: towards the central axis or outwards from the central axis); (b) magnetic flux density. (For interpretation of the references to color in this figure legend, the reader is referred to the web version of this article.)

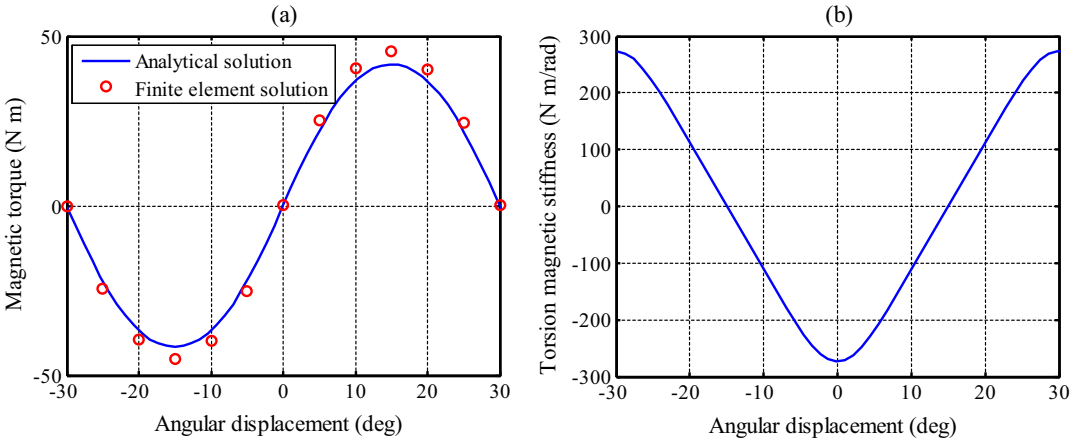

Fig. 4. (a) Representation of the magnetic torque versus the angular displacement, both analytical solution and finite element solution are given; (b) representation of the magnetic stiffness versus the angular displacement. B_r = 1.3 T, N = 12, R_{i2} = 15 mm, T_2 = 15 mm, G = 5 mm, T_1 = 15 mm, L = 40 mm, $\lambda_1 = \lambda_2 = 1$.

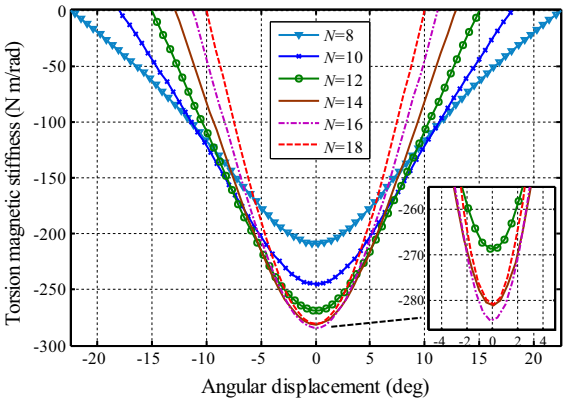

Fig. 5. Effect of the number of poles on the torsion magnetic stiffness. B_r = 1.3 T, R_{i2} = 15 mm, T_2 = 15 mm, G = 5 mm, T_1 = 15 mm, L = 40 mm, $\lambda_1 = \lambda_2 = 1$.

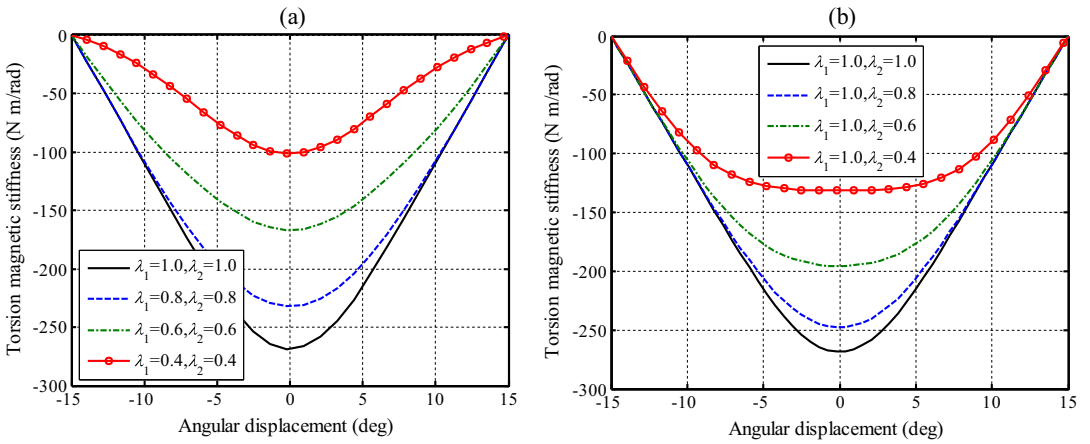

Fig. 6. Effect of the angular width of tile magnets on the torsion magnetic stiffness: (a) effect of the absolute values of λ_1 and λ_2; (b) effect of the difference between λ_1 and λ_2. B_r = 1.3 T, N = 12, R_{i2} = 15 mm, T_2 = 15 mm, G = 5 mm, T_1 = 15 mm, L = 40 mm.

to decrease the nonlinearity of stiffness and increase the effective stroke length. The loss of negative stiffness can be compensated as required by other methods, which will be introduced in the following section.

3.3. Effect of the air gap (G)

As shown in Fig. 7, the TMS possesses strong soften-stiffness nonlinearity around the equilibrium position when the air gap is small. This can lead to jumping phenomenon in the vibration transmissibility of the coupling, also it will make it impossible to match the positive stiffness of the rubber spring and attain quasi-zero stiffness at the equilibrium position, or the total stiffness around the equilibrium position will become negative and the system will be statically unstable. When the air gap is increased, the magnetic stiffness about the equilibrium position would become more uniform. But the cost is that the value of negative stiffness is decreased significantly due to the increase of magnetic leakage. Thus appropriate air gap should be chosen to guarantee both the value of negative stiffness and its uniformity in the designing process. Besides, too small an air gap will bring great difficulty to the manufacturing and mounting process, which also needs to be taken into consideration.

3.4. Effect of the inner radii of inner tiles (R_{i2}), radial thickness (T_1, T_2) and length (L) of tile magnets

Figs. 8–10 describe the effect of the parameters (R_{i2}, T_1, T_2, L) on the stiffness characteristic, which indicates that it is effective to increase the value of negative stiffness by increasing these parameters. On the other hand, the extent of linearity around the equilibrium point is nearly not affected when these parameters vary, which is a beneficial characteristic for designing the TMS. When determining these parameters, the size of the TMS needs to be weighed against the value of neg-

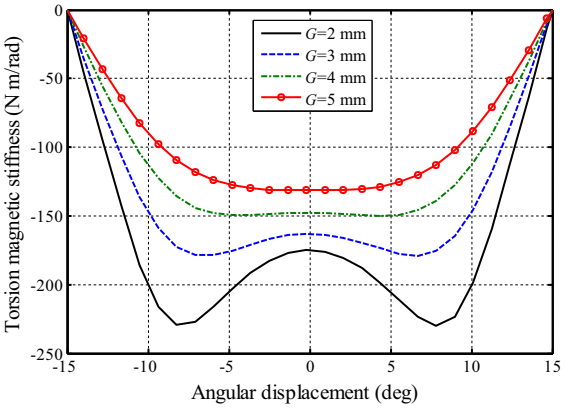

Fig. 7. Effect of the air gap between the inner magnet and outer magnet on the torsion magnetic stiffness. B_r = 1.3 T, N = 12, R_{i2} = 15 mm, T_2 = 15 mm, T_1 = 15 mm, L = 40 mm, $\lambda_1 = 1$, $\lambda_2 = 0.4$.

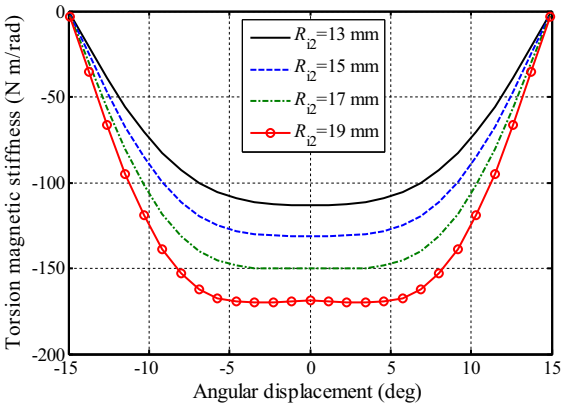

Fig. 8. Effect of the inner radii of inner magnet arrangement on the torsion magnetic stiffness. B_r = 1.3 T, N = 12, T_2 = 15 mm, G = 5 mm, T_1 = 15 mm, L = 40 mm, $\lambda_1 = 1$, $\lambda_2 = 0.4$.

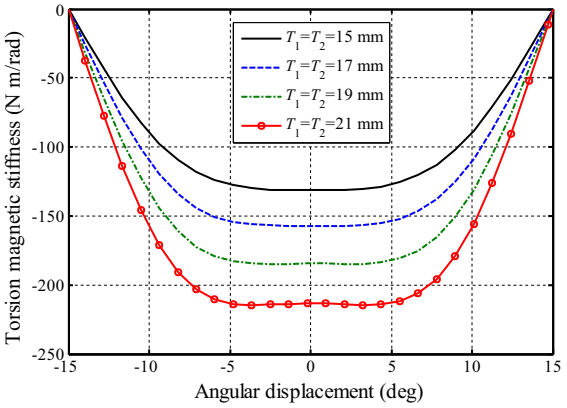

Fig. 9. Effect of the radial thickness of tile magnets on the torsion magnetic stiffness. B_r = 1.3 T, N = 12, R_{i2} = 15 mm, G = 5 mm, L = 40 mm, $\lambda_1 = 1$, $\lambda_2 = 0.4$.

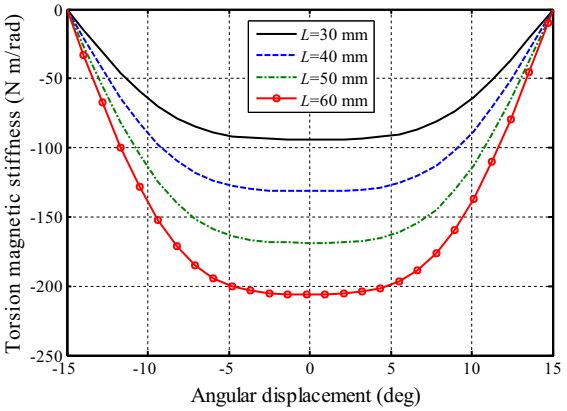

Fig. 10. Effect of the length of tile magnets on the torsion magnetic stiffness. B_r = 1.3 T, N = 12, R_{i2} = 15 mm, T_2 = 15 mm, G = 5, T_1 = 15 mm, $\lambda_1 = 1$, $\lambda_2 = 0.4$.

ative stiffness, especially if the coupling is applied to precision equipment where the size is usually an important evaluating factor.

Based on the analysis from Section 3.1–3.4, some rules can be followed when designing the TMS. Firstly, the number of poles should be appropriate: large enough to produce large negative stiffness and not too large to keep the structure simple. Secondly, increasing the inner radii of the inner tiles, the radial thickness and the axial length of tiles is a good choice if the

value of negative stiffness needs to be increased; the size of the coupling should be balanced with the negative stiffness when designing these parameters. Finally, increasing the air gap and the difference of angular width between the inner tiles and the outer tiles can make the stiffness around the equilibrium position more uniform.

4. Dynamic analysis of the quasi-zero stiffness (QZS) coupling

4.1. The total torque and stiffness of the coupling

The achieved expressions of the magnetic torque and stiffness of the torsion magnetic spring (TMS) in Appendix A are integral, which are not convenient for analysis of the dynamic equation. Hence it is necessary to approximate the torque and stiffness with simple expressions such as the polynomial. The procedure to approximate the torque and stiffness is as follows: firstly the magnetic torque and stiffness are calculated employing the integral expressions in Appendix A; and then the total torque and stiffness are acquired using Eqs. (1) and (2); finally the total stiffness is approximated by a polynomial and the total torque is obtained by integrating the polynomial of total stiffness. Since the total stiffness is an even function of θ, it can be approximated by the polynomial presented as

$$K(\theta) = \sum_{i=0}^{n} k_i \theta^{2i} \tag{3}$$

Accordingly, the expression of the total torque can be obtained as

$$M(\theta) = \sum_{i=0}^{n} a_i \theta^{2i+1} \tag{4}$$

where $a_i = k_i/(2i+1)$. If the order number $(2n)$ of the total stiffness is large enough, the approximate solution will be close to the exact solution.

The stiffness of the rubber spring is chosen to be 150 N m/rad; the residual flux density of magnets is 1.3 T and geometric parameters of the TMS are designed as Table 1 where four cases are considered. Then the total stiffness and torque of the coupling are calculated as Fig. 11. Here the 6-order polynomials are adopted to approximate the total stiffness and demonstrate good coincidence with the exact solutions. The coefficients of the 6-order polynomial are given as Table 2.

Table 1
Geometric parameters of the torsion magnetic spring (TMS).

Cases	N	λ_1	λ_2	R_{i2}/mm	T_2/mm	G/mm	T_1/mm	L/mm
TMS 1	12	1.0	0.4	15	16	5	16	40
TMS 2	12	1.0	1.0	15	10	5	10	40
TMS 3	12	1.0	0.4	15	10	2	10	40
TMS 4	12	1.0	0.4	15	10	5	10	40

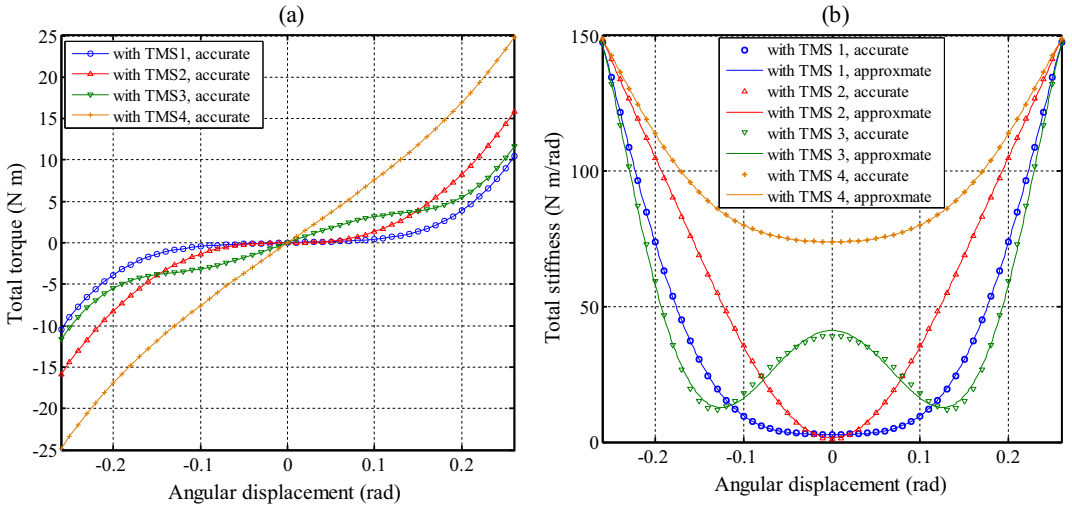

Fig. 11. Static characteristics of the coupling with torsion magnetic spring (TMS): (a) total torque versus angular displacement; (b) total stiffness versus angular displacement, and the accurate stiffness is approximated by a 6-order polynomial curve.

Table 2
Coefficients of the 6-order polynomial for the total stiffness of the coupling.

Cases	k_0/N m rad^{-1}	k_1/N m rad^{-3}	k_2/N m rad^{-5}	k_3/N m rad^{-7}
With TMS 1	2.8	1.8×10^2	5.5×10^4	-3.9×10^5
With TMS 2	1.6	3.7×10^3	-3.7×10^4	2×10^5
With TMS 3	41	-3.9×10^3	1.5×10^5	-9.7×10^5
With TMS 4	74	4.5×10^2	1.9×10^4	-1.4×10^5

As shown in Table 1, for TMS 1, the radial thickness of the inner tiles and the outer tiles is increased compared with TMS 4. For TMS 4, the difference of angular width between the inner tiles and the outer tiles is increased compared with TMS 2 and the air gap is increased compared with TMS 3. Accordingly, the total stiffness of the couplings with different TMS varies as Fig. 11(b): the one with TMS 1 has the best stiffness characteristics since its equilibrium position approach the state of quasi-zero stiffness and the stiffness keeps nearly constant in the range of -0.1–0.1 rad; the one with TMS 2 possesses quasi-zero stiffness at the equilibrium position but it has the characteristics of harden stiffness and the stiffness nonlinearity is strong; the one with TMS 3 has the characteristics of soften stiffness; the one with TMS 4 possesses relatively large stiffness at the equilibrium position though its stiffness nonlinearity is weak. In the following, it will be analyzed in detail how the geometric parameters of the TMS influence the stiffness characteristic and hence the isolation performance of the coupling.

4.2. Dynamic equation

The main function of the coupling is to transmit the driving torque from the driving shaft to the driven shaft. Ideally, the driving torque is constant, which can be seen as a static load for the coupling. But actually the driving torque will be accompanied by a disturbing component $M_d \cos(\omega t + \alpha)$, which can also be transmitted to the driven shaft and then influence the rotor system. The QZS coupling proposed in this paper is employed to suppress the disturbing torque transmitted to the driven shaft while transmitting the static driving torque smoothly. To evaluate the isolation performance of the proposed isolator, the torque transmissibility of the isolator needs to be considered.

The angular displacement of the motor is θ_1 and that of the rotor is θ_2, hence the relative angular displacement between the inner magnet arrangement and the outer one is $\theta = \theta_1 - \theta_2$. The moment of inertia of the motor is I_1 and that of the rotor is I_2. The viscous damping torque $c\dot{\theta}$ is assumed. Then the dynamic equation of the system is expressed as

$$\begin{cases} I_1 \cdot \theta_1 + c \cdot \theta + M(\theta) = M_d \cos(\omega t + \alpha) \\ I_2 \cdot \theta_2 - c \cdot \theta - M(\theta) = 0 \end{cases} \tag{5}$$

Eq. (5) can be transformed to

$$\frac{I_2}{I_1 + I_2} \cdot I_1 \cdot \ddot{\theta} + c \cdot \theta + M(\theta) = \frac{I_2}{I_1 + I_2} \cdot M_d \cos(\omega t + \alpha) \tag{6}$$

Letting

$$\kappa = I_2/(I_1 + I_2), \quad I = \kappa \cdot I_1, \quad M_0 = \kappa \cdot M_d \tag{7}$$

Eq. (6) can be simplified as

$$I \cdot \ddot{\theta} + c \cdot \dot{\theta} + M(\theta) = M_0 \cos(\omega t + \alpha) \tag{8}$$

where $M(\theta)$ is given by Eq. (4). It is beneficial to nondimensionalize the proceeding dynamic equation as

$$\varphi''(\tau) + 2\zeta\varphi'(\tau) + \sum_{i=0}^{n} \delta_i \varphi^{2i+1} = m_0 \cos(\beta\tau + \alpha) \tag{9}$$

where

$$\begin{aligned} &\varphi = \frac{\theta}{\gamma}, \quad \omega_n = \sqrt{\frac{K_r}{I}}, \quad \tau = \omega_n t, \quad \zeta = \frac{c}{2I\omega_n} \\ &m_0 = \kappa \cdot m_d, \quad m_d = \frac{M_d}{K_r \gamma}, \quad \beta = \frac{\omega}{\omega_n}, \quad \delta_i = \frac{a_i}{K_r} \gamma^{2i} \end{aligned} \tag{10}$$

γ is the reference for the nondimensionalization of θ.

For the nonlinear dynamic equation Eq. (9), the Harmonic Balance Method is usually employed to acquire its approximate solution [42]. The initial phase of the disturbing torque α is chosen to be such that the solution can be assumed to be

$$\varphi = \phi \cos(\beta\tau) \tag{11}$$

Substituting Eq. (11) into Eq. (9), it can be derived that

$$-\beta^2 \phi \cos(\beta\tau) - 2\zeta\beta\phi \sin(\beta\tau) + \sum_{i=0}^{n} \delta_i \phi^{2i+1} \cos^{2i+1}(\beta\tau) = m_0 \cos(\beta\tau + \alpha) \tag{12}$$

As for the term $\cos^{2i+1}(\beta\tau)$, it can be approximated by its first-order harmonic component $1/2^{2i}\cdot C_{2i+1}^{i+1}\cos(\beta\tau)$. Then Eq. (12) can be transformed to

$$\begin{cases} -\beta^2\phi+\lambda = m_0\cos\alpha \\ 2\zeta\beta\phi = m_0\sin\alpha \end{cases} \tag{13}$$

with

$$\lambda = \sum_{i=0}^{n} 1/2^{2i}\cdot C_{2i+1}^{i+1}\delta_i\phi^{2i+1} \tag{14}$$

Solving Eq. (13) can deduce the relation between ϕ and β, expressed as

$$\beta^2 = \frac{\lambda-2\phi\zeta^2 \pm \sqrt{4\zeta^4\phi^2-4\lambda\phi\zeta^2+m_0^2}}{\phi} \tag{15}$$

The amplitude of the dimensionless torque transmitted to the driven shaft is

$$m_b = \sqrt{(2\zeta\beta\phi)^2+\lambda^2} \tag{16}$$

Hence the torque transmissibility is

$$T = \frac{\sqrt{(2\zeta\beta\phi)^2+\lambda^2}}{m_d} \tag{17}$$

The relation between the transmissibility T and the dimensionless frequency β can be gained by employing Eqs. (15) and (17).

In Section 4.1, it is stated that the order number of the polynomial employed to approximate the total stiffness is not definite. Whatever the order number is, the derivation procedure of the torque transmissibility is the same with that given above. The only difference is the variable λ. For the stiffness characteristic shown as Fig. 11, which is approximated by a sixth order polynomial, the variable λ can then be expressed as

$$\lambda = \delta_0\phi+\frac{3}{4}\delta_1\phi^3+\frac{5}{8}\delta_2\phi^5+\frac{35}{64}\delta_4\phi^7 \tag{18}$$

4.3. Isolation performance of the quasi-zero stiffness (QZS) coupling

It is convenient to employ the analytical expression of the torque transmissibility shown as Eq. (17) to study the isolation performance of the coupling. The analytical results are achieved by the first-order harmonic balance method; but the subharmonic and super-components usually exist for nonlinear systems, which may have great influence on the dynamic response and hence reduce the precision of the analytical results. Hence the analytical transmissibility is verified by comparing it with the numerical results firstly.

The damping ratio ζ is specified as 0.005. Assuming that $I_2/I_1 \gg 1$, the parameter κ then equals to 1 and the achieved results will not lose generality. The amplitude of the disturbing torque is set to be $m_d = 0.005$ in the simulation, which is the largest value adopted in the following analytical calculation. The numerical analysis of Eq. (9) is performed using the ode45 solver of MATLAB. The simulation time is long enough to ensure that the dynamic response can reach the steady state. Then the root mean square of the torque $\overline{m}_b(t)$ transmitted to the driven shaft and that of the disturbing torque $\overline{m}_d(t)$ are calculated in a time interval of the steady state, where

$$\begin{aligned} \overline{m}_b(\tau) &= 2\zeta\varphi'(\tau)+\sum_{i=0}^{n}\delta_i\varphi^{2i+1} \\ \overline{m}_d(\tau) &= m_d\cos(\beta\tau+\alpha) \end{aligned} \tag{19}$$

And the torque transmissibility obtained by the numerical method can then be expressed as [50]

$$T_n = \frac{RMS(\overline{m}_b(t))}{RMS(\overline{m}_d(t))} \tag{20}$$

Both forward and backward frequency-weep analysis are conducted. Fig. 12 shows that the numerical results are in good agreement with the analytical results in the whole frequency range. Thus the analytical expressions of the torque transmissibility can be employed in the following study.

The torque transmissibility of the coupling with different TMS as presented in Table 1 will be studied to evaluate its isolation performance. For nonlinear isolators, the jumping phenomenon may occur and thus reduce its effective isolation fre-

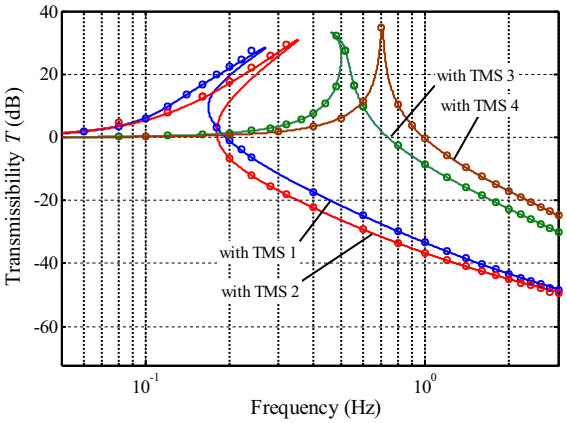

Fig. 12. Comparing of the transmissibility obtained by Harmonic balance method (solid line) and numerical method (circle points): four cases with different torsion magnetic springs (TMS).

quency band and deteriorate the isolation performance. Thus the isolation performance of the coupling will be evaluated from two aspects: the resonance frequency and the jumping phenomenon.

As shown in Fig. 11(b), for the coupling with TMS 1, its stiffness in the range of −0.1 to 0.1 rad is low and nearly constant and this range can be seen as the effective stroke length of the QZS coupling. As shown in Fig. 13, the frequency response curve bends to the right due to the harden-spring characteristics; the peak of the displacement amplitude increases as the disturbing torque increases and accordingly the transmissibility curve bends to the right more severely due to the stronger nonlinearity. When the disturbing torque is $m_d = 0.001$, the peak of the displacement amplitude is lower than 0.1 rad and the jumping phenomenon does not appear; the isolation frequency band of the coupling with TMS 1 is much larger than that without TMS. As m_d increases to 0.002, the peak of the displacement amplitude is a little larger than 0.1 rad and the jumping phenomenon emerges; but the jump-down frequency is still lower than the critical frequency where the transmissibility is 0 dB, which means that the jumping phenomenon does not influence the isolation frequency band. As m_d increases further to 0.003 or be larger, the jump-down frequency exceeds the critical frequency and thus the effective isolation frequency band is reduced. The analysis above demonstrates that the stiffness nonlinearity of the QZS coupling is weak in the range of −0.1 to 0.1 rad and the coupling can works well in this range. The isolation performance of the couplings with TMS 2 and TMS 3 will also be evaluated in this range and compared with that of the coupling with TMS 1.

The stiffness of the coupling with TMS 2 is highly nonlinear about the equilibrium position though it attains the quasi-zero stiffness state. As shown in Fig. 14, the frequency response curves present strong nonlinearity in all cases. When the disturbing torque is 0.001 and 0.002, the peak of the displacement amplitude is limited to be lower than 0.1 rad; but the jump-down frequency still surpasses the critical frequency and hence reduces the effective isolation frequency band. So the coupling with TMS 2 cannot works well in the range of −0.1 to 0.1 rad due to the strong stiffness nonlinearity.

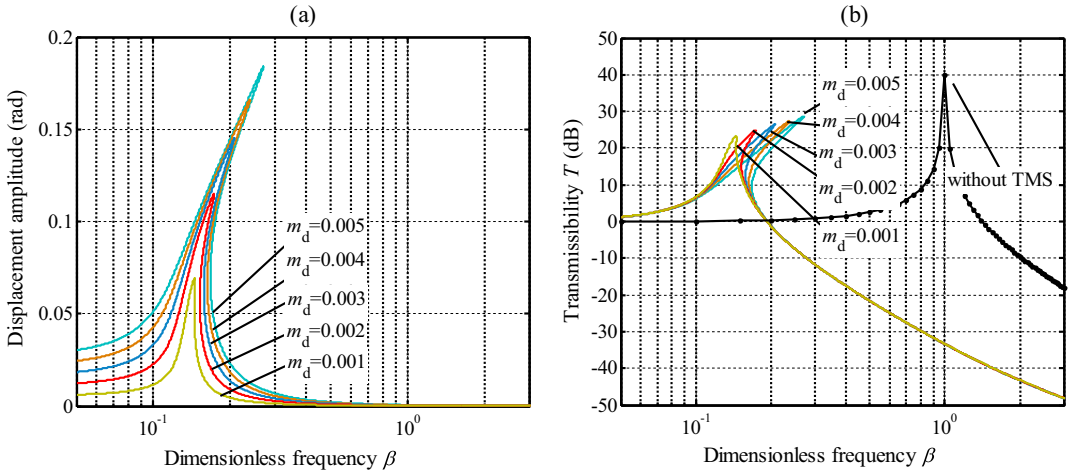

Fig. 13. Frequency response of the coupling with torsion magnetic spring 1 (TMS 1) under different disturbing torques: (a) amplitude of the angular displacement; (b) torque transmissibility.

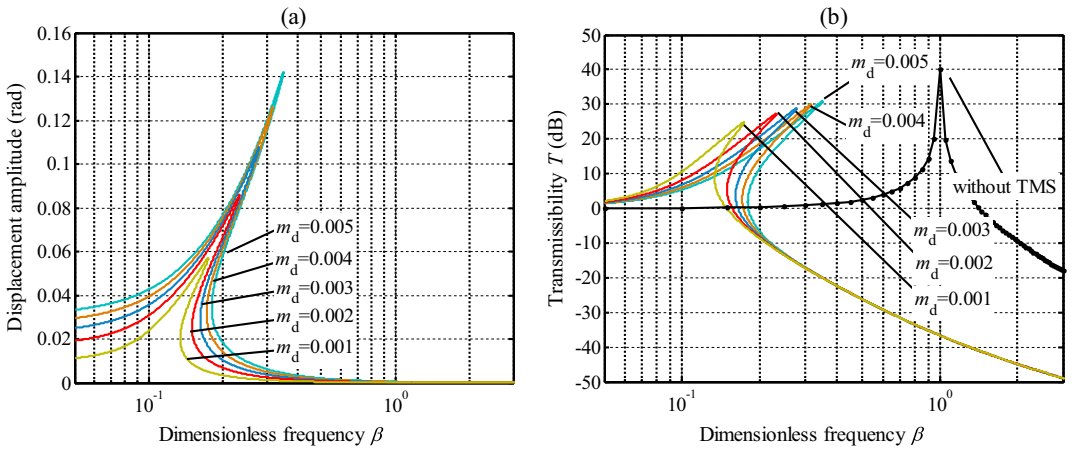

Fig. 14. Frequency response of the coupling with torsion magnetic spring 2 (TMS 2) under different disturbing torques: (a) amplitude of the angular displacement; (b) torque transmissibility.

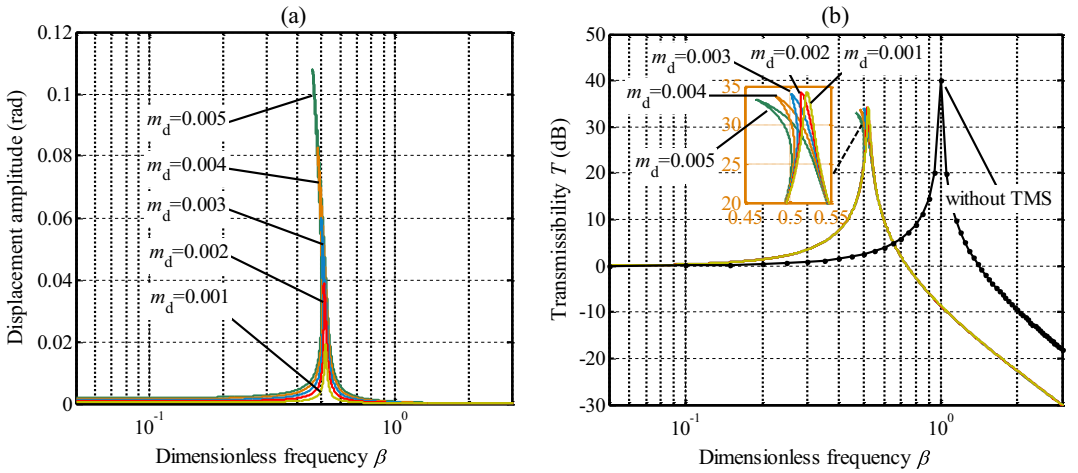

Fig. 15. Frequency response of the coupling with torsion magnetic spring 3 (TMS 3) under different disturbing torques: (a) amplitude of the angular displacement; (b) torque transmissibility.

As shown in Fig. 15, the frequency response curves of the coupling with TMS 3 bends to the left due to the soften-stiffness characteristics. Though it does not affect the effective isolation frequency band, the stiffness at the equilibrium position is required to be large to ensure positive stiffness around the equilibrium position. Thus the resonance frequency is high and the isolation frequency band is narrow compared with that of the coupling with TMS 1.

Since the isolation performance of the coupling with TMS 2 and TMS 3 is not as fine as that with TMS 1 in the range of −0.1 to 0.1 rad, it is necessary to optimize the stiffness characteristic of the TMS to improve the isolation performance. The optimization procedure can be concluded from Section 3, and the torque transmissibility of the couplings with TMS 1 ∼ TMS 4, as shown in Fig. 16, can help present the effect of the optimization.

For the coupling with TMS 2, by increasing the difference of angular width between the inner tiles and outer tiles, stiffness nonlinearity can be reduced and hence the jumping phenomenon can be avoided. This can be seen from the comparing of the transmissibility of the coupling with TMS 2 and that with TMS 4. But the disadvantage is that the resonance frequency is boosted to a high level and the isolation frequency band is reduced. For the coupling with TMS 3, the air gap of TMS 3 can be increased to decrease its soften-stiffness nonlinearity. Fig. 16 shows that the transmissibility of the coupling with TMS 3 does not present strong nonlinearity compared to that with TMS 4 though the air gap is smaller, which is due to the high stiffness at the equilibrium position. Since the harden-stiffness nonlinearity of TMS 2 (or soften-stiffness nonlinearity of TMS 3) has been decreased, several measures proposed in Section 3 can be taken to increase the negative magnetic stiffness and reduce the resonance frequency. Here the measure of increasing radial thickness is taken and its effect can be revealed from the transmissibility with TMS 1 and that with TMS 4.

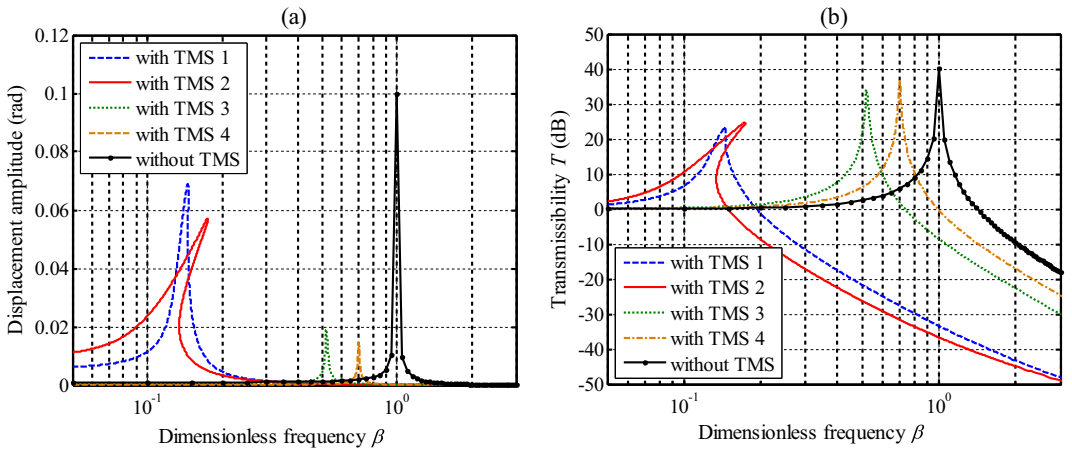

Fig. 16. Frequency response of the coupling with different torsion magnetic springs (TMS) when $m_d = 0.001$: (a) amplitude of the angular displacement; (b) torque transmissibility.

5. Conclusions

In this paper, a novel quasi-zero stiffness (QZS) coupling is proposed, which is mainly composed of a rubber spring and a torsion magnetic spring (TMS). The TMS could produce negative stiffness to cancel the positive stiffness of the rubber spring about the equilibrium position. The QZS coupling can isolate disturbing torque in a wide frequency band due to its low dynamic stiffness. Since the static torque is undertaken by the rubber, which has high stiffness, the QZS coupling can maintain a small static angular displacement when a large driving torque is transmitted through it. This can be a great advantage when it is applied in shaft systems that require isolating disturbing torque while transmitting large static driving torque.

In order to design an appropriate TMS, the effect of geometric parameters on the stiffness characteristic is analyzed from three aspects: the value of negative stiffness, the extent of nonlinearity and the stroke length. The results indicate that by optimizing the geometric parameters it is possible to gain large and flat negative stiffness in a wide stroke length around the equilibrium point. The dynamic equation is then established and the analytical expression of the torque transmissibility is derived. The obtained torque transmissibility proves that the QZS coupling can have a good isolation performance in its effective stroke length and also shows how the geometric parameters of the TMS can influence the isolation performance of the coupling.

Acknowledgments

This work was supported by the National Natural Science Foundation of China (Grant No. 11172225).

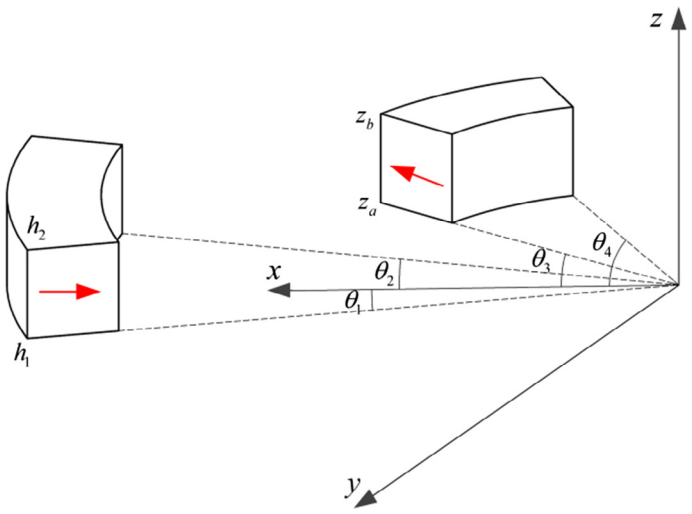

Fig. A1. Schematic for calculating the magnetic torque between the inner tile magnet and the outer tile magnet.

Appendix A. Analytical expressions of the torque and torsion stiffness of the magnetic spring

For the torsion magnetic spring (TMS) proposed in this paper, the inner ring magnet arrangement and the outer one are in a repulsive configuration. The reference [46] gives the expression of magnetic torque produced by two tile magnets arranged as Fig. A.1. Hence, for the presented TMS, the magnetic torque produced by the ith inner tile and the jth outer tile can be given as

$$\begin{aligned} M_{ij}(\theta) = -\Bigg(& \int_{\theta_3}^{\theta_4} (M_1^{(R_{o1},R_{o2})} - M_1^{(R_{i1},R_{o2})} + M_1^{(R_{i1},R_{i2})} - M_1^{(R_{o1},R_{i2})}) d\theta_i + \int_{\theta_3}^{\theta_4} \int_{R_{i1}}^{R_{o1}} (M_2^{(r_1,R_{i2})} - M_2^{(r_1,R_{o2})}) dr_1 d\theta_i \\ & + \int_{\theta_3}^{\theta_4} \int_{R_{i2}}^{R_{o2}} (M_3^{(R_{i1},r_2)} - M_3^{(R_{o1},r_2)}) dr_2 d\theta_i + \int_{\theta_3}^{\theta_4} \int_{R_{i1}}^{R_{o1}} \int_{R_{i2}}^{R_{o2}} M_4^{(r_1,r_2)} dr_1 dr_2 d\theta_i \Bigg) \end{aligned} \tag{A.1}$$

with

$$\begin{aligned} M_1^{(a,b)} &= -\frac{a^2 b^2 \sigma_1 \sigma_2}{4\pi\mu_0} (g(\theta_2) - g(\theta_1)) \\ M_2^{(a,b)} &= -\frac{a b^2 \sigma_1 \sigma_2}{4\pi\mu_0} (g(\theta_2) - g(\theta_1)) \\ M_3^{(a,b)} &= -\frac{a^2 b \sigma_1 \sigma_2}{4\pi\mu_0} (g(\theta_2) - g(\theta_1)) \\ M_4^{(a,b)} &= -\frac{a b \sigma_1 \sigma_2}{4\pi\mu_0} (g(\theta_2) - g(\theta_1)) \end{aligned} \tag{A.2}$$

and

$$\begin{aligned} g(\theta_j) &= \beta(a,b,h_2,z_a,\theta_i,\theta_j) - \beta(a,b,h_1,z_a,\theta_i,\theta_j) \\ &\quad + \beta(a,b,h_1,z_b,\theta_i,\theta_j) - \beta(a,b,h_2,z_b,\theta_i,\theta_j) \\ \beta(a,b,z_a,z_b,a,b,\theta_i,\theta_j) &= -\frac{\eta}{ab} \arctan\left(\frac{\xi}{\eta}\right) + \frac{\xi}{ab} \\ \xi &= \sqrt{a^2 + b^2 + (z_2 - z_1)^2 - 2ab\cos(\theta_i - \theta_j)} \\ \eta &= \sqrt{-(z_1 - z_2)^2} \end{aligned} \tag{A.3}$$

where σ_1 and σ_2 are the magnetic pole surface density, $\sigma_1 = \sigma_2 = B_r$; B_r is the residual magnetic flux density of the magnets and μ_0 is the permeability of the vacuum; the geometric parameters in the above expressions can be found in Fig. 2 and Fig. A.1; $h_1 = 0$, $h_2 = L$, $z_a = 0$, $z_b = L$; $\theta_1, \theta_2, \theta_3, \theta_4$ can be obtained as functions of the angular displacement θ of the TMS. It should be noted that if the magnetization directions of the ith tile and jth tile are the same, the expression Eq. (A.1) should be reversed. The total torque of the magnetic spring can then be expressed as

$$M_m(\theta) = \sum_{i=1}^{N} \sum_{j=1}^{N} M_{ij}(\theta) \tag{A.4}$$

The magnetic stiffness generated between the ith inner tile and the jth outer tile is derived as

$$K_{ij}(\theta) = -\frac{dM_{ij}(\theta)}{d\theta} \tag{A.5}$$

According to Eq. (A.1), M_{ij} can be simplified as

$$M_{ij} = \int_{\theta_3}^{\theta_4} f(\theta_i) d\theta_i \tag{A.6}$$

where $f(\theta_i)$ is an integral expression. Substituting Eq. (A.6) into Eq. (A.5), it can be derived that

$$\begin{aligned} K_{ij}(\theta) &= -\frac{\int_{\theta_3+d\theta}^{\theta_4+d\theta} f(\theta_i) d\theta_i - \int_{\theta_3}^{\theta_4} f(\theta_i) d\theta_i}{d\theta} \\ &= -\frac{f(\theta_4) d\theta - f(\theta_3) d\theta}{d\theta} \\ &= f(\theta_3) - f(\theta_4) \end{aligned} \tag{A.7}$$

Since $K_{ij}(\theta)$ is known, the total magnetic stiffness can then be obtained as

$$K_m(\theta) = \sum_{i=1}^{N} \sum_{j=1}^{N} K_{ij}(\theta) \tag{A.8}$$

The expressions of the magnetic torque and stiffness shown as Eqs. (A.1)–(A.7) are integral, which can be solved by the method of numerical integration.

References

[1] R.S. Lakes, Extreme damping in composite materials with a negative stiffness phase, Phys. Rev. Lett. 86 (2001) 2897–2900.
[2] R.S. Lakes, T. Lee, A. Bersie, Y.C. Wang, Extreme damping in composite materials with negative-stiffness inclusions, Nature 410 (2001) 565–567.
[3] T. Jaglinski, D. Kochmann, D. Stone, R.S. Lakes, Composite materials with viscoelastic stiffness greater than diamond, Science 315 (2007) 620–622.
[4] L. Dong, R. Lakes, Advanced damper with high stiffness and high hysteresis damping based on negative structural stiffness, Int. J. Solids Struct. 50 (2013) 2416–2423.
[5] M.R. Haberman, T.D. Klatt, P.S. Wilson, C. Seepersad, Negative stiffness metamaterials and periodic composites, J. Acoust. Soc. Am. 131 (2012) 3372.
[6] T. Klatt, M.R. Haberman, A nonlinear negative stiffness metamaterial unit cell and small-on-large multiscale material model, J. Appl. Phys. 114 (2013) 033503.
[7] S.P. Pellegrini, N. Tolou, M. Schenk, J.L. Herder, Bistable vibration energy harvesters: a review, J. Intell. Mater. Syst. Struct. 24 (2013) 1303–1312.
[8] R.L. Harne, K.W. Wang, A review of the recent research on vibration energy harvesting via bistable systems, Smart Mater. Struct. 22 (2013) 023001.
[9] K. Avramov, Y.V. Mikhlin, Snap-through truss as a vibration absorber, J. Vib. Control 10 (2004) 291–308.
[10] K.V. Avramov, Y.V. Mikhlin, Snap-through truss as an absorber of forced oscillations, J. Sound Vib. 290 (2006) 705–722.
[11] D.R. Johnson, R.L. Harne, K.W. Wang, A Disturbance cancellation perspective on vibration control using a bistable snap-through attachment, J. Vib. Acoust. 136 (2014), 031006-031006-031008.
[12] L.I. Manevitch, G. Sigalov, F. Romeo, L.A. Bergman, A. Vakakis, Dynamics of a linear oscillator coupled to a bistable light attachment: analytical study, J. Appl. Mech. 81 (2013), 041011-041011-041019.
[13] F. Romeo, G. Sigalov, L.A. Bergman, A.F. Vakakis, Dynamics of a linear oscillator coupled to a bistable light attachment: Numerical study, J. Comput. Nonlinear Dyn. 10 (2015) 011007.
[14] H. Yao, Z. Chen, B. Wen, Dynamic vibration absorber with negative stiffness for rotor system, Shock Vib. 2016 (2016).
[15] J. Zhao, X. Li, Y. Wang, W. Wang, B. Zhang, X. Gai, Membrane acoustic metamaterial absorbers with magnetic negative stiffness, J. Acoust. Soc. Am. 141 (2017) 840–846.
[16] J. Zhou, K. Wang, D. Xu, H. Ouyang, Local resonator with high-static-low-dynamic stiffness for lowering band gaps of flexural wave in beams, J. Appl. Phys. 121 (2017) 044902.
[17] F. Weber, C. Boston, M. Maślanka, An adaptive tuned mass damper based on the emulation of positive and negative stiffness with an MR damper, Smart Mater. Struct. 20 (2011) 015012.
[18] Y. Shen, X. Wang, S. Yang, H. Xing, Parameters optimization for a kind of dynamic vibration absorber with negative stiffness, Math. Probl. Eng 2016 (2016).
[19] Y. Shen, H. Peng, X. Li, S. Yang, Analytically optimal parameters of dynamic vibration absorber with negative stiffness, Mech. Syst. Signal Process. 85 (2017) 193–203.
[20] M.A. Acar, C. Yilmaz, Design of an adaptive–passive dynamic vibration absorber composed of a string–mass system equipped with negative stiffness tension adjusting mechanism, J. Sound Vib. 332 (2013) 231–245.
[21] D.L.Platus, Negative-stiffness-mechanism vibration isolation systems, in: Proceedings of SPIE1619, Vibration Control in Microelectronics, Optics, and Metrology, 1991, pp. 44–54.
[22] X. Huang, X. Liu, J. Sun, Z. Zhang, H. Hua, Vibration isolation characteristics of a nonlinear isolator using Euler buckled beam as negative stiffness corrector: a theoretical and experimental study, J. Sound Vib. 333 (2014) 1132–1148.
[23] X. Huang, Y. Chen, H. Hua, X. Liu, Z. Zhang, Shock isolation performance of a nonlinear isolator using Euler buckled beam as negative stiffness corrector: theoretical and experimental study, J. Sound Vib. 345 (2015) 178–196.
[24] X. Liu, X. Huang, H. Hua, On the characteristics of a quasi-zero stiffness isolator using Euler buckled beam as negative stiffness corrector, J. Sound Vib. 332 (2013) 3359–3376.
[25] A. Carrella, M.J. Brennan, T.P. Waters, Static analysis of a passive vibration isolator with quasi-zero-stiffness characteristic, J. Sound Vib. 301 (2007) 678–689.
[26] A. Carrella, M.J. Brennan, I. Kovacic, T.P. Waters, On the force transmissibility of a vibration isolator with quasi-zero-stiffness, J. Sound Vib. 322 (2009) 707–717.
[27] T.D. Le, K.K. Ahn, Experimental investigation of a vibration isolation system using negative stiffness structure, Int. J. Mech. Sci. 70 (2013) 99–112.
[28] T.D. Le, K.K. Ahn, A vibration isolation system in low frequency excitation region using negative stiffness structure for vehicle seat, J. Sound Vib. 330 (2011) 6311–6335.
[29] C.-C. Lan, S.-A. Yang, Y.-S. Wu, Design and experiment of a compact quasi-zero-stiffness isolator capable of a wide range of loads, J. Sound Vib. 333 (2014) 4843–4858.
[30] D. Xu, Y. Zhang, J. Zhou, J. Lou, On the analytical and experimental assessment of the performance of a quasi-zero-stiffness isolator, J. Vib. Control 20 (2014) 2314–2325.
[31] A. Carrella, M.J. Brennan, T.P. Waters, K. Shin, On the design of a high-static–low-dynamic stiffness isolator using linear mechanical springs and magnets, J. Sound Vib. 315 (2008) 712–720.
[32] K. Shin, On the performance of a single degree-of-freedom high-static-low-dynamic stiffness magnetic vibration isolator, Int. J. Precis. Eng. Manuf. 15 (2014) 439–445.
[33] N. Zhou, K. Liu, A tunable high-static–low-dynamic stiffness vibration isolator, J. Sound Vib. 329 (2010) 1254–1273.
[34] W. Wu, X. Chen, Y. Shan, Analysis and experiment of a vibration isolator using a novel magnetic spring with negative stiffness, J. Sound Vib. 333 (2014) 2958–2970.
[35] Y. Shan, W. Wu, X. Chen, Design of a miniaturized pneumatic vibration isolator with high-static-low-dynamic stiffness, J. Vib. Acoust. 137 (2015) 045001.
[36] Y. Zheng, X. Zhang, Y. Luo, B. Yan, C. Ma, Design and experiment of a high-static–low-dynamic stiffness isolator using a negative stiffness magnetic spring, J. Sound Vib. 360 (2016) 31–52.
[37] Y. Araki, K. Kimura, T. Asai, T. Masui, T. Omori, R. Kainuma, Integrated mechanical and material design of quasi-zero-stiffness vibration isolator with superelastic Cu–Al–Mn shape memory alloy bars, J. Sound Vib. 358 (2015) 74–83.
[38] W.S. Robertson, M.R.F. Kidner, B.S. Cazzolato, A.C. Zander, Theoretical design parameters for a quasi-zero stiffness magnetic spring for vibration isolation, J. Sound Vib. 326 (2009) 88–103.
[39] T. Zhu, B. Cazzolato, W.S.P. Robertson, A. Zander, Vibration isolation using six degree-of-freedom quasi-zero stiffness magnetic levitation, J. Sound Vib. 358 (2015) 48–73.
[40] X. Sun, X. Jing, Multi-direction vibration isolation with quasi-zero stiffness by employing geometrical nonlinearity, Mech. Syst. Signal Process. 62–63 (2015) 149–163.
[41] J. Zhou, X. Wang, D. Xu, S. Bishop, Nonlinear dynamic characteristics of a quasi-zero stiffness vibration isolator with cam–roller–spring mechanisms, J. Sound Vib. 346 (2015) 53–69.
[42] J. Zhou, D. Xu, S. Bishop, A torsion quasi-zero stiffness vibration isolator, J. Sound Vib. 338 (2015) 121–133.
[43] J.P. Yonnet, Permanent magnet bearings and couplings, IEEE Trans. Magn. 17 (1981) 1169–1173.

[44] J.P. Yonnet, S. Hemmerlin, E. Rulliere, G. Lemarquand, Analytical calculation of permanent magnet couplings, IEEE Trans. Magn. 29 (1993) 2932–2934.
[45] E.P. Furlani, R. Wang, H. Kusnadi, A three-dimensional model for computing the torque of radial couplings, IEEE Trans. Magn. 31 (1995) 2522–2526.
[46] R. Ravaud, G. Lemarquand, V. Lemarquand, C. Depollier, Permanent magnet couplings: field and torque three-dimensional expressions based on the coulombian model, IEEE Trans. Magn. 45 (2009) 1950–1958.
[47] X. Huang, X. Liu, J. Sun, Z. Zhang, H. Hua, Effect of the system imperfections on the dynamic response of a high-static-low-dynamic stiffness vibration isolator, Nonlinear Dyn. 76 (2014) 1157–1167.
[48] X.C. Huang, X.T. Liu, H.X. Hua, Effects of stiffness and load imperfection on the isolation performance of a high-static-low-dynamic-stiffness non-linear isolator under base displacement excitation, Int. J. Non-Linear Mech. 65 (2014) 32–43.
[49] Y. Araki, T. Asai, K. Kimura, K. Maezawa, T. Masui, Nonlinear vibration isolator with adjustable restoring force, J. Sound Vib. 332 (2013) 6063–6077.
[50] Z. Lu, M.J. Brennan, L.-Q. Chen, On the transmissibilities of nonlinear vibration isolation system, J. Sound Vib. 375 (2016) 28–37.